Three-dimensional printing of mycelium hydrogels into living complex materials

Gantenbein, Silvan; Colucci, Emanuele; Käch, Julian; Trachsel, Etienne; Coulter, Fergal B.; Rühs, Patrick A.; Masania, Kunal; Studart, André R.

DOI
10.1038/s41563-022-01429-5

Publication date
2022

Document Version
Final published version

Published in
Nature Materials

Citation (APA)
Gantenbein, S., Colucci, E., Käch, J., Trachsel, E., Coulter, F. B., Rühs, P. A., Masania, K., & Studart, A. R. (2022). Three-dimensional printing of mycelium hydrogels into living complex materials. *Nature Materials*, *22*(1), 128-134. https://doi.org/10.1038/s41563-022-01429-5

nature materials

Article

https://doi.org/10.1038/s41563-022-01429-5

Three-dimensional printing of mycelium hydrogels into living complex materials

Received: 7 June 2021

Accepted: 2 November 2022

Published online: 22 December 2022

Check for updates

Silvan Gantenbein[1], Emanuele Colucci[1], Julian Käch[1], Etienne Trachsel[1], Fergal B. Coulter[1], Patrick A. Rühs[1], Kunal Masania[1,2] ✉ & André R. Studart[1] ✉

Biological living materials, such as animal bones and plant stems, are able to self-heal, regenerate, adapt and make decisions under environmental pressures. Despite recent successful efforts to imbue synthetic materials with some of these remarkable functionalities, many emerging properties of complex adaptive systems found in biology remain unexplored in engineered living materials. Here, we describe a three-dimensional printing approach that harnesses the emerging properties of fungal mycelia to create living complex materials that self-repair, regenerate and adapt to the environment while fulfilling an engineering function. Hydrogels loaded with the fungus *Ganoderma lucidum* are three-dimensionally printed into lattice architectures to enable mycelial growth in a balanced exploration and exploitation pattern that simultaneously promotes colonization of the gel and bridging of air gaps. To illustrate the potential of such mycelium-based living complex materials, we three-dimensionally print a robotic skin that is mechanically robust, self-cleaning and able to autonomously regenerate after damage.

Living organisms have long been exploited to synthesize materials for engineering needs, such as silk, cellulose and wood[1,2], and have also led to materials with enhanced functionalities[3]. This strategy has gained new inspiration in recent years, motivated by the sustainable nature of biological processes and the possibility of creating synthetic materials with living functionalities through the incorporation of microorganisms in abiotic host matrices[4–10]. The combination of material-producing microorganisms with abiotic synthetic building blocks has led to the development of self-healing concretes for construction[4,11], antibiotic-releasing living surfaces[6], genetically programmable living materials for sensing[5,7] and biomedical applications[8], as well as functional living inks for three-dimensional (3D) printing of bacteria-laden materials[9,12]. The ability to program microorganisms using synthetic biological tools[2,7,8] and to 3D print living inks into intricate geometries[7,9] potentially designed by artificial intelligence[13] opens enticing perspectives in the growing field of engineered living materials[14,15].

Among the different microorganisms exploited so far, a fungal mycelium is particularly interesting because it is a living, complex, adaptive system with emergent collective properties[16–20]. Such complex behaviour results from the fact that fungal mycelia have evolved to explore and exploit environments with distributed patches of nutrients either as decomposers or as symbionts with plants. To optimally gather these nutrients, mycelia form large networks consisting of interconnected elongated cells, each called a hypha. The hyphae locally absorb water and nutrients and use them to power mycelial exploration of the surroundings or the formation of fruiting bodies for even further dissemination. These features make mycelia a fascinating biological example of a complex adaptive system comprising a network of decentralized units (cells) that self-organize into hierarchical structures with emerging collective behaviour[16]. In fungal mycelia, adaptation to the environment is manifested by its ability to change growth patterns between the exploratory and exploitation strategies according to the local availability of nutrients. Such adaptive behaviour gives rise

[1]Complex Materials, Department of Materials, ETH Zürich, Zürich, Switzerland. [2]Present address: Shaping Matter Lab, Faculty of Aerospace Engineering, Delft University of Technology, Delft, Netherlands. ✉e-mail: K.Masania@tudelft.nl; andre.studart@mat.ethz.ch

to growth, communication and decision-making properties that are highly desired in synthetic materials.

Several approaches have been pursued to exploit mycelium-based materials for engineering purposes. A mycelium grown on agricultural waste acts as a binder to create sustainable materials that have been commercialized as environmentally friendly boards for insulation and packaging[21]. Mycelial structures have also been fabricated for architectural applications[22], as leather-like self-grown films with tunable mechanical properties[23,24], as scaffolds in the biomedical field[25] or as biological templates to synthesize inorganic filaments[26]. However, the fungi utilized for the fabrication of all these materials and products eventually die at the end of the process or are removed from the structure, which thereby does not benefit from the unique adaptive living properties of the microorganisms.

Here, we combine the emerging adaptive behaviour of mycelial networks with the capability of shaping matter in three dimensions to create mycelium-based, living, complex materials that serve specific engineering purposes. Because the living organism has evolved for a biological function, harnessing its emerging properties for other applications requires one to shape the organisms into new structures. To address this, we print open architectures that provide a 3D environment for the growth of mycelia into a functional complex material, outside of the host hydrogel. The amount of nutrients available is deliberately controlled to enable the mycelium-based living material to find the right exploration–exploitation balance needed for the mycelia to grow, self-regenerate and autonomously adapt in response to the environment.

Printing of living hydrogels

Living complex materials were 3D printed using hydrogels inoculated with mycelia. The workflow involves mixing an agar-based hydrogel containing malt extract and rheology modifiers to obtain a granulated ink, the deposition of the fungus on top of such granular inks and finally the removal of the fungus top layer to create the mycelium-laden feedstock for 3D printing via direct ink writing (Fig. 1a). The feedstock ink is printed into mechanically stable grid-like architectures that provide the open space and the nutrients required for the mycelia to grow. Incubation of the printed object at ambient temperature and high relative humidity allows for the growth of the mycelia both within and between the deposited filaments without the drying of the hydrogel structure.

The shaping capabilities of 3D printing can be exploited to manufacture complex materials in geometries that match the functional requirements of specific engineering scenarios. One possible embodiment of this concept is to create protective living skins for robots. To fulfil this function, the skin should be mechanically robust but also sufficiently active to allow for self-regeneration of damaged sites. Such apparently contradicting features can be achieved by 3D printing mycelium-laden hydrogels into engineered structures that would otherwise not exist in the natural world (Fig. 1b). In these structures, mechanical robustness arises from the formation of a strong fibrous mycelial network with a shape that is relevant for the final application. The livingness and the ability to self-regenerate damaged sites emerges from the metabolic activity of the mycelial cells, which have evolved in nature to navigate through and grow within the openings of porous structures. The ultimate function of the living complex material is eventually fulfilled through a unique hierarchical architecture that spans from the individual mycelium cells to the hyphal network and grid-like structures shaped into designer macroscopic geometries (Fig. 1b).

Fungal growth

To create the proposed mycelium-based, living, complex material, we first identified the conditions required for the preparation of printable mycelial hydrogels and for fungal growth between the gaps expected in the grid-like structures. The processing conditions leading to hydrogel inks with high mycelial concentrations were evaluated by studying the growth behaviour of the fungus deposited on top of an agar-based hydrogel substrate (Fig. 2a,b and Extended Data Fig. 1a,b). To this end, a rectangular piece of fungi inoculum was placed onto the substrate surface and grown at 23 °C and a relative humidity of 95% (Supplementary Information). Growth was quantified by measuring the radial and thickness expansions of the fungus after a fixed period of five days upon deposition on hydrogels with distinct initial concentrations of malt extract. The results indicate that mycelial growth is strongly affected by the concentration of malt extract available in the substrate (Fig. 2b). Low concentrations favour radial expansion of the fungus with limited growth of thickness of the mycelium layer on the surface. The radial growth of fungi placed on gels with malt extract contents of 2–4% is around 65% larger compared to those cultured on top of gels with 15–20% malt extract. Instead of radial expansion, fungi deposited on hydrogels containing these high malt extract contents tend to grow thicker layers on the gel. Indeed, our data reveal that the fungus grows 1.7-times-thicker mats on the hydrogel when the initial malt extract concentration changes from 2 to 14%.

The distinct growth forms observed can be interpreted in terms of the balance between exploration and exploitation used by diverse species of fungi and plants[17–19]. When exposed to high concentrations of readily available nutrients, mycelia utilize an exploitation growth strategy known as phalanx. In this case, the organism advances slowly in a united front, leading to the formation of highly branched and dense hypha mats. By contrast, mycelium growth switches to an exploration form called guerilla if the local availability of nutrients is low. Such a scenario induces the organism to opportunistically search for nutrients, resulting in far-reaching hyphae with a low level of branching. For the mycelium species utilized in this work, a compromise between exploration and exploitation is found at an intermediate malt extract concentration of 10%, at which the volume of fungus is approximately two times larger than the levels reached at lower and higher malt contents (Extended Data Fig. 1c). Because of this balanced exploration–exploitation strategy, a mycelium cultured with this optimum nutrient concentration not only grows locally within the hydrogel but is also able to bridge air gaps of up to 2.5 mm at an average growth velocity of 0.20–0.35 mm day^{-1} (Fig. 2c,d).

The 3D printing of complex-shaped grids is possible by turning the fungal growth media with the intermediate content of malt extract (10%) into aqueous inks displaying rheological properties suitable for direct ink writing. For grid-like structures, the printing inks should display a sufficiently high storage modulus to prevent filament sagging and a high yield stress to minimize capillarity- and gravity-driven shape distortions. Using oscillatory rheology, we found that the inoculation of the base ink with mycelia does not alter its viscoelastic properties (the storage (G') and loss (G'') moduli) at shear strains below 1% (Fig. 2e). However, shear stress–strain measurements reveal that the presence of mycelia increases the yield stress of the base ink from around 400 Pa to nearly 700 Pa (Fig. 2f). Our rheological characterization suggests that the viscoelastic properties at low shear strains are dominated by the constituents of the base hydrogel, whereas the mycelial network plays a mechanical strengthening role that is activated only at higher deformations. Importantly, the storage modulus and the yield stress of the mycelium inks are sufficient to minimize the filament sagging and distortions resulting from capillary or gravitational forces (Extended Data Fig. 2 and Supplementary Note).

Printing and mechanics of grids

Mycelium-laden inks with optimal rheological properties were 3D printed into stable grid-like architectures using a desktop extrusion-based printer. Grids with distinct filament spacings, diameters and malt extract concentrations were prepared using different ink formulations and programmable printing paths (Extended Data Fig. 3). Incubation of these printed grids for up to 20 days allowed for the effective growth of mycelia between the hydrogel filaments, leading to

https://doi.org/10.1038/s41563-022-01429-5

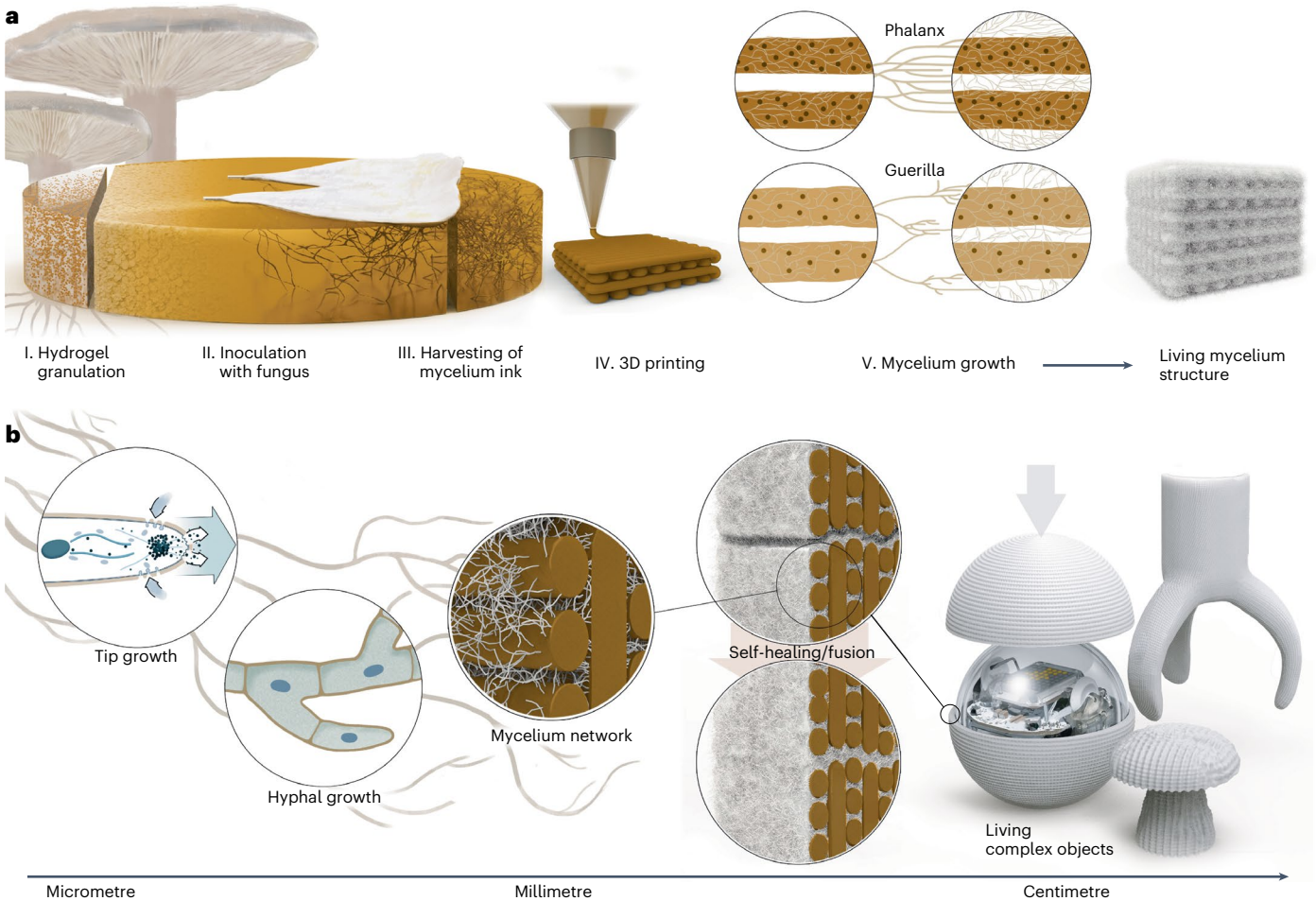

Fig. 1 | Living complex materials and objects made by 3D printing of mycelium-laden hydrogels. a, Schematics displaying the distinct steps of the 3D-printing process, from the preparation of inks with inoculated mycelia (left), to the direct ink writing of mycelial hydrogels into grid architectures (middle), to the growth of the fungus through the phalanx or guerrilla strategy depending on the nutrient concentration (right). **b**, Hierarchical structure of the resulting mycelium-based objects, highlighting (from left to right) the cell-level growth through self-organization processes, the hyphal cells that form the mycelial network, the growth of the mycelial network between printed hydrogel filaments, the self-healing and regeneration processes across large air gaps and the macroscopic geometry of the complex material according to the shapes that are relevant for the final applications.

mechanically robust living structures (Fig. 3a,b and Extended Data Fig. 1). The growth of the mycelia over time was quantified by measuring the relative amount of dry biomass left after grinding and extensively washing the grid in water. The results show that the dry mass of mycelia is initially zero and grows linearly up to about 4–5 wt% within the first ten days of incubation, after which the amount of biomass was found to level off (Fig. 3c). This behaviour indicates that the malt concentration of 10% used in these experiments is sufficient to induce steady mycelial growth in the first ten days, but the nutrients are eventually depleted from the culture medium after this time window.

The growth of mycelia between the filaments results in a robust fungal-based living material that is highly resistant to tearing, stretching and compression compared to the initial hydrogel-based grid (Supplementary Video 1). We quantify the stiffness of the grid by performing compression experiments on specimens incubated for different time periods (Fig. 3). Typical stress–strain curves obtained from these measurements reveal a continuous stiffening of the grid as the applied strain is increased. Taking the slope of the stress–strain data as the instantaneous elastic modulus of the material (Fig. 3d), we found that the grid undergoes sequential stiffening processes upon uniaxial compression. In situ imaging indicates that adjacent filaments along the height of the sample remain separated by the mycelia during the first stiffening process but are eventually pushed into one another when the second stiffening event takes place. As compression and densification proceed, the grid continues to stiffen sharply until it eventually fractures, which is accompanied by a sudden burst of liquid from the sample (Extended Data Fig. 4 and Supplementary Video 1).

To better understand the role of the fungal network on the mechanical properties of the mycelium-based living material, we measured the elastic modulus of the grid as a function of growth time (Fig. 3e). With a steady increase in the first ten days of incubation, the stiffness of the grid directly reflects the growth curve of the mycelial network. Indeed, the measured stiffness was observed to scale directly with the amount of dry biomass produced by the microorganism (Fig. 3f). This suggests that the elastic modulus of the complex material is determined by the load-bearing capacity of the mycelial network formed between the filaments of the grid. The direct correlation between the stiffness of the grid and the dry biomass produced also helps explain the effects of the malt extract concentration and of the line gap on the elastic modulus of the grid (Fig. 3g,h). For grids prepared with different malt concentrations, we found that an excess of nutrients does not necessarily lead to a higher concentration of biomass within the grid. This finding might correlate with the fact that high sugar contents reduce the water activity[27], which has been shown to decrease the growth of filamentous fungi[28].

https://doi.org/10.1038/s41563-022-01429-5

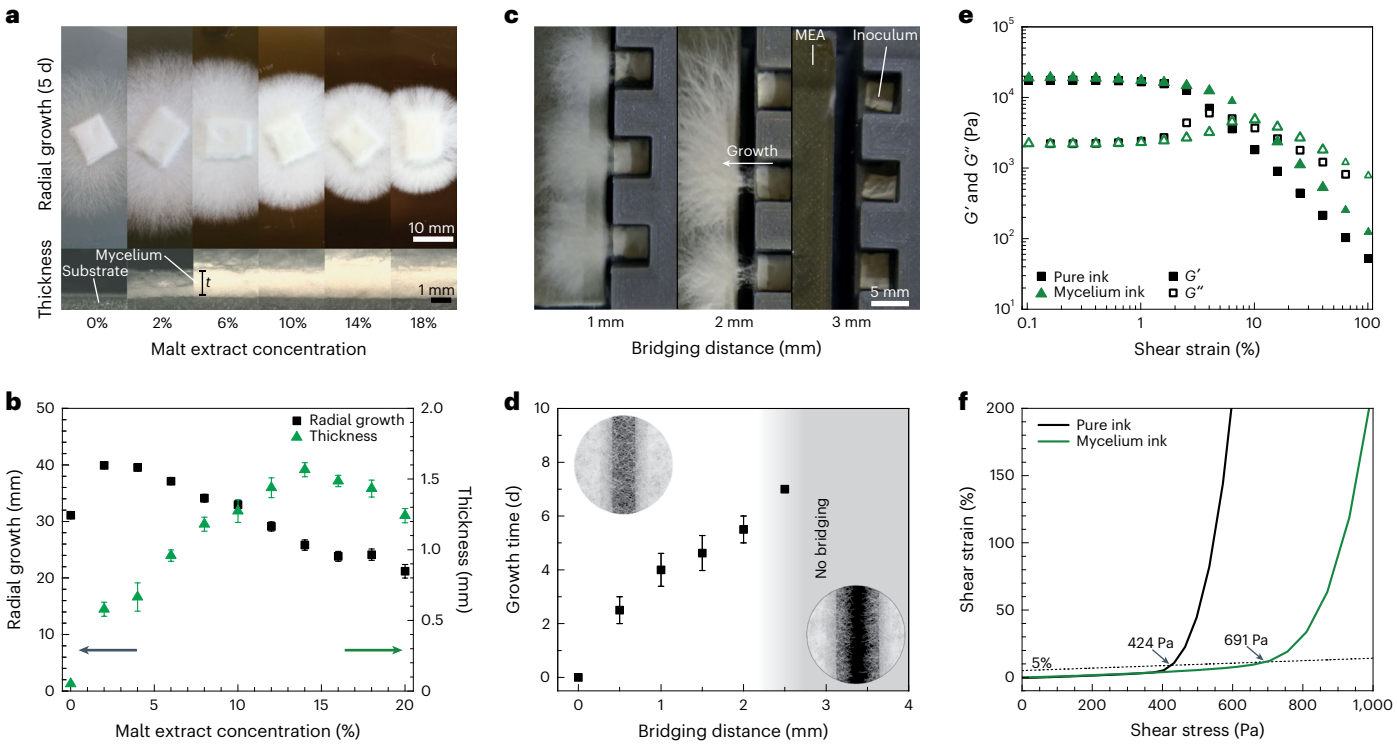

Fig. 2 | Fungal growth behaviour and rheology of mycelium-laden hydrogels. **a**,**b**, Growth in radius and thickness (t) after five days of mycelia inoculated on the surface of agar gels containing varying concentrations of malt extract. The rectangular samples consist of pieces of agar hydrogel with pre-inoculated mycelia. The data shown in **b** represent the mean values obtained from five different samples. **c**,**d**, Bridging of mycelia across air gaps intentionally formed between the surface of inoculated agar gels. The time that it takes for the mycelia to bridge an air gap of defined length is shown in the plot (**d**). The data represent the mean values obtained from five different samples. **e**, Storage (G') and loss (G'') moduli of mycelium-laden hydrogel ink as a function of the applied oscillatory strain. **f**, Flow behaviour of the mycelium-laden hydrogel ink, highlighting the yield stress below which no substantial deformation takes place. The rheological behaviour of a mycelium-free ink is also shown in **e** and **f** for comparison. Error bars represent the standard deviation of five measurements of distinct samples at each data point.

Living and self-regenerating behaviour

The metabolic activity of the mycelial network endows our 3D-printed objects with remarkable living and self-regenerating properties. We illustrate these properties by first studying the growth behaviour of the microorganism across physically separated surfaces and air gaps in model experiments (Fig. 4a–c and Supplementary Video 2). To gain insight into the livingness of our material, the mycelial network that grows between two fungi-laden hydrogel filaments was imaged over time in a laser scanning confocal microscope (Fig. 4b). In this set-up, two ink filaments were printed 1.2 mm apart onto a glass slide and covered with another thin glass slide, leaving an air gap in between. The mycelial network that grows from the surface of the filament was detected using a fluorescent dye (calcofluor white) that specifically adsorbs onto the chitin molecules present in the walls of the hypha cells.

Confocal images of the mycelia formed in the air gap between the printed filaments reveal that the microorganisms form a fractal-like network during growth under the conditions of the experiment. Such fractal morphology is typically characterized by a decrease in the number of cells (N) with the distance from the filament surface (L), as expressed by the scaling relation $N \propto L^{D/3}$, where D is the fractal dimension. By assuming the fluorescence intensity to be an indirect measure of the cell number and fitting this equation to our experimental intensity data, we estimate a fractal dimension that lies between 1.16 and 1.50 for the mycelial network grown for two to five days. These values fall within the typical range of mycelial networks, which may vary from 1 for organisms that grow by the guerrilla strategy to 2 for fungi with the phalanx growth form[29]. The fact that the fractal dimension obtained from our image analysis lies closer to 1 reflects the strong guerrilla growth characteristics and exploratory nature of our mycelial network.

The exploratory nature of the fungal network is key to enabling the regeneration of damaged areas of the mycelium-based living material, damage caused by its interactions with the environment. To demonstrate this self-regenerating capability, we introduced cuts of different sizes in a piece of living mycelial film and measured the distance travelled by the growing front as a function of time for specimens prepared with different malt extract concentrations (Fig. 4c). The results show that the mycelia grow at a speed in the range 0.6–0.7 mm day^{-1} after an initial lag phase, to reach a maximum healing distance of 2.5 to 3 mm, if the malt concentration is equal or higher than the threshold value of 6%. This size range is comparable to the defect size of 5 mm typically used to study self-healing processes that take place during regeneration of fractured human bone[30]. While the availability of nutrients is crucial to enable self-regeneration and sustain life, viability experiments show that the mycelial network can be brought back from a dormant to a metabolically active state even after the material has been depleted from culture medium in the hydrated or dried state for as many as eight months (Extended Data Fig. 5). Moreover, the fungi generated after this dormant phase are able to outcompete other microorganisms, such as yeast, during the regrowth phase. This impressive resilience preserves the livingness of the mycelial network even in very adverse environments and conditions.

To evaluate whether such a self-healing effect also enables recovery of the mechanical properties of the mycelium-based living material, we measured the tensile strength and elastic modulus of dog-bone-shaped specimens before and after successive fracture–healing events (Fig. 4d and Supplementary Video 3). Considering the

https://doi.org/10.1038/s41563-022-01429-5

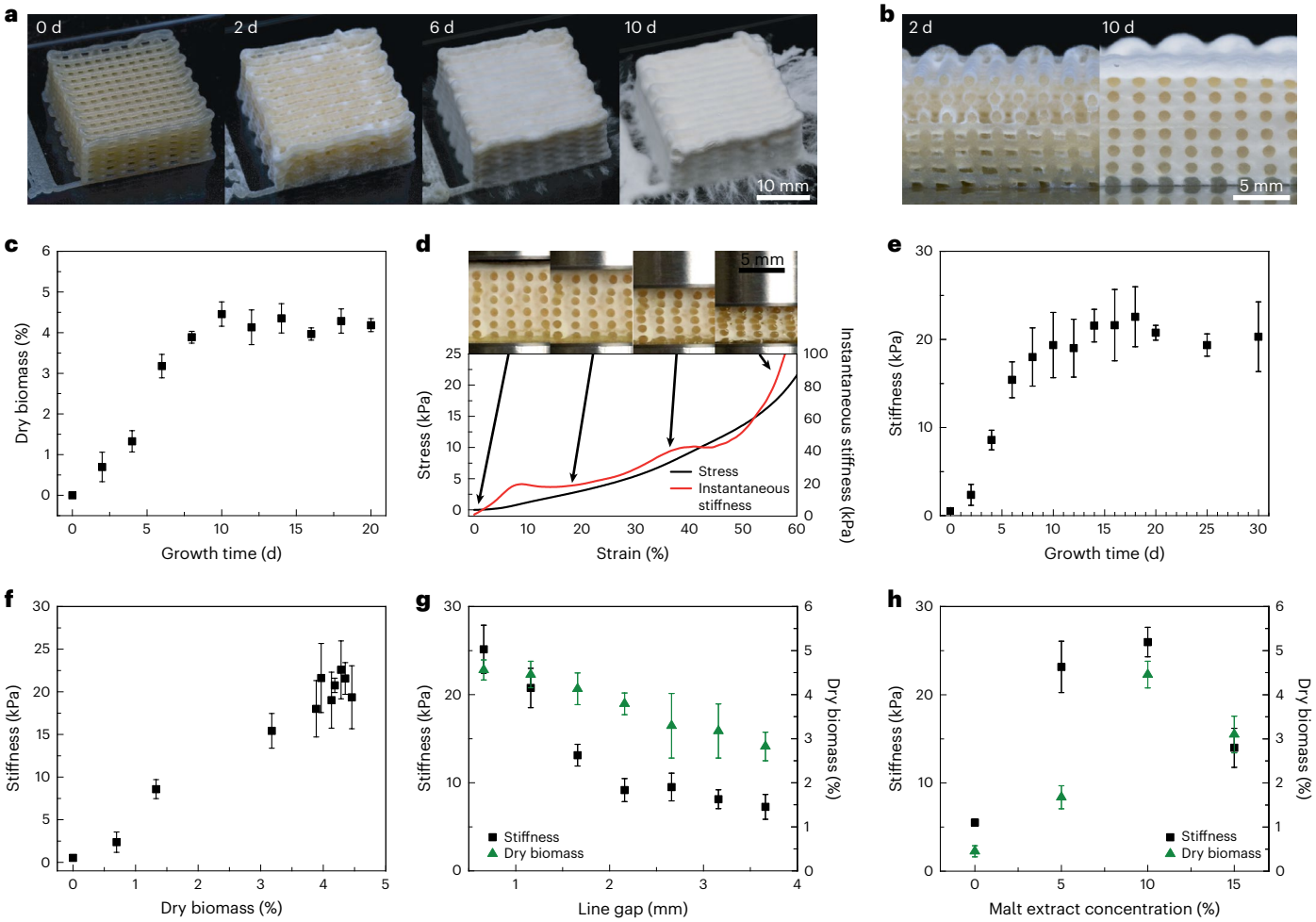

Fig. 3 | Growth and mechanical stiffness of mycelium-based living material with 10% malt concentration. a, Photographs of the 3D-printed mycelium-based grids with increasing growth times. **b**, Cross-section of the grid after two and ten days of incubation, indicating the notable growth of mycelia in between the printed hydrogel filaments. **c**, Amount of biomass generated by the fungus as a function of time for grids printed with a line spacing of 2 mm and using a nozzle diameter of 0.84 mm (as shown in **a** and **b**). The data represent the mean values obtained from five different samples. **d**, Representative stress–strain curve obtained from the mechanical compression tests (black line) and the associated variation in instantaneous stiffness (red line). The insets show in situ images of the cross-section of the material at different applied strain levels. **e**, Apparent stiffness as a function of growth time for mycelium-containing grids printed with a line spacing of 2 mm and using a nozzle diameter of 0.84 mm (shown in **a** and **b**). **f**, Correlation between the apparent stiffness and the biomass concentration of grids shown in **a** and **b**. **g**,**h**, Apparent stiffness and biomass content of mycelium-laden grids printed with different gaps between the grid lines (**g**) and with hydrogels containing distinct malt extract concentrations (**h**). The apparent stiffness values reported in **e**–**h** correspond to the instantaneous elastic modulus at a strain value of 25%. The data represent the mean values and the standard deviation obtained from five measurements of distinct samples at each data point.

living nature of the material, the experiments were carried out during the growth phase of the mycelial network. Remarkably, the fractured complex material is able to self-heal into stronger and stiffer structures, as long as the mycelial network has sufficient nutrients to grow across the fractured surfaces. In fact, the network formed across fractured surfaces was observed to be strong enough to shift the fracture site to another location of the sample in a subsequent healing cycle (Fig. 4e). After the initial growth phase, the healed material still maintains a high elastic modulus but fails at much lower stresses. In addition to self-healing the damaged sites of a given object, we found that the mycelia are also able to grow across the air gaps between separate objects positioned next to one another (Extended Data Fig. 6a). This enables the creation of complex-shaped living structures by simply joining individual parts that were manufactured separately (Fig. 4f).

Living mycelia as robotic skin

The livingness and printability of the mycelium-based hydrogel opens the possibility to create functional structures with bespoke designs and unprecedented adaptive behaviour. As illustrative examples, we 3D printed our mycelium-based living material in the form of self-regenerating functional skins for a robotic gripper and for an untethered rolling robot (Fig. 4g–i). Following the strategy described earlier, the skins are manufactured by printing the mycelium-laden hydrogel into a grid-like architecture that conforms to the geometry of the gripper's arms and of the spherical shape of the rolling robot (Extended Data Fig. 7). After growth, the skin is sufficiently robust to keep its mechanical integrity and living nature while being exposed to the high frictional forces required to move the rolling robot on a variety of different surfaces (Fig. 4i and Supplementary Video 4). Moreover, the hydrophobic character of the mycelial network prevents wetting of the skin by water, providing waterproof self-cleaning capabilities to the rolling robot. We demonstrate this additional feature by designing an experiment in which the skin-covered gripper and rolling robot work cooperatively to enable programmed underwater motion (Fig. 4j and Supplementary Video 5). Our experiments reveal that the hydrophobic nature of the skin prevents

https://doi.org/10.1038/s41563-022-01429-5

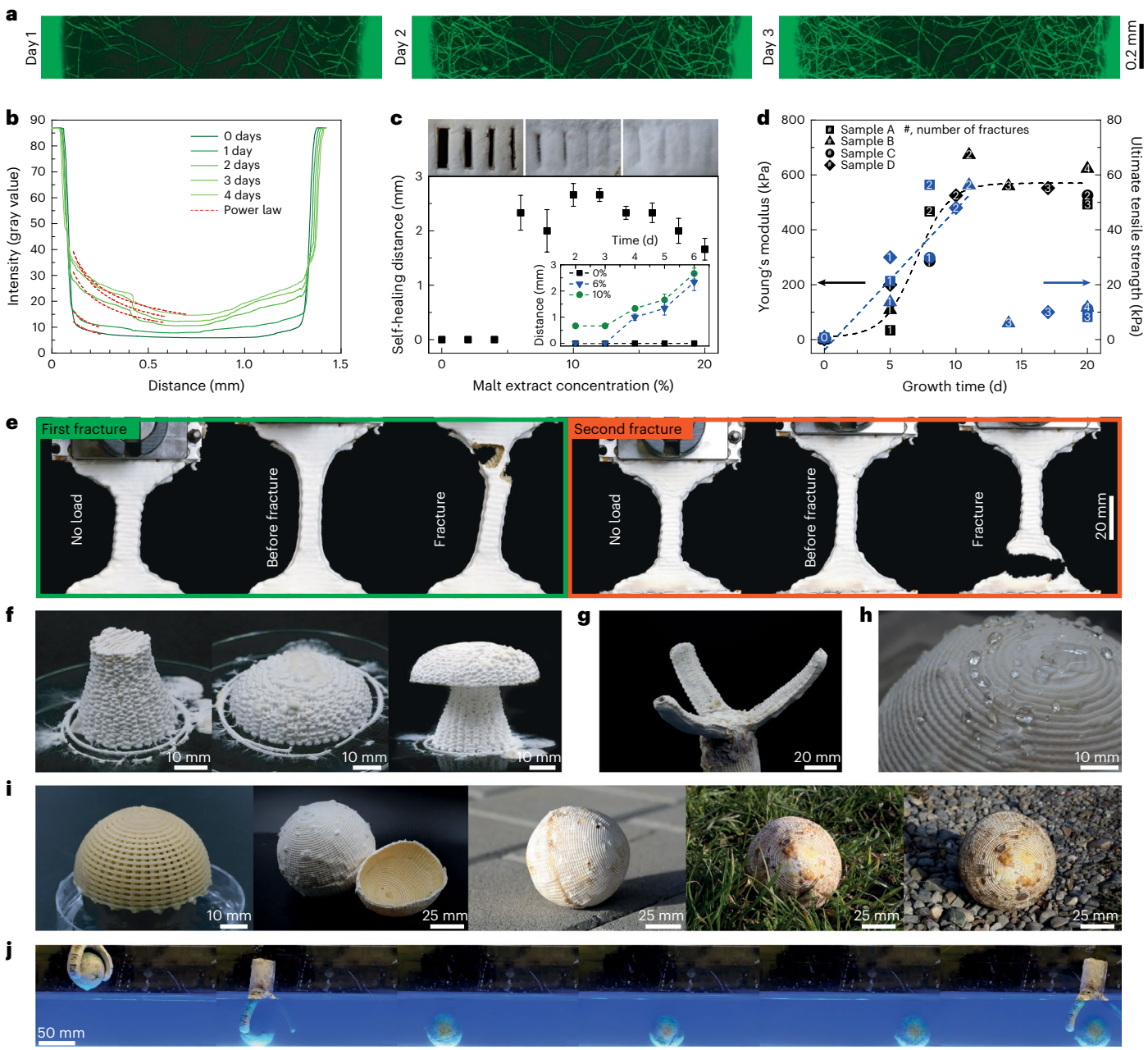

Fig. 4 | Livingness, self-healing and application of mycelium-based living materials. a, Laser confocal microscopy images of dyed mycelia (green) growing between two hydrogel filaments printed 1.2 mm apart. These images are representatives of a series of three experiments. **b**, Intensity profiles of the images shown in **a** quantifying the time evolution of the spatial distribution of the mycelial network grown between the two filaments. The decay in fluorescence intensity as a function of distance is fitted with a power law to demonstrate the scale-free nature of the network. **c**, Self-healing distance covered by the mycelia across a cut deliberately introduced into a mycelium-containing film prepared with different malt extract concentrations. The pictures shown as insets display a film with 10% malt extract after two, four and six growth days. The distance healed by the mycelia over time is also included as an inset for specimens with selected malt extract concentrations. The data represent the mean values and the standard deviation obtained from five measurements of distinct samples at each data point. **d**, Young's modulus and the ultimate strength of samples subjected to multiple fracture–healing cycles during growth of the mycelium-based living material. **e**, Photographs of the tensile mechanical tests performed to demonstrate the self-healing ability of the mycelium-based material. **f**, Joining of 3D-printed parts into a single object through the growth of mycelia between surfaces in physical contact. **g**,**h**, Living skins printed on top of a robotic gripper (**g**) and an untethered rolling robot (**h**). Water droplets on the surface of the skin illustrate the hydrophobic nature of the mycelium-based living material. **i**, Snapshots of the skin covering the rolling robot before and after mycelial growth. Photographs of the rolling robot after friction-driven locomotion on different surfaces demonstrate the mechanical robustness of the living skin. **j**, Snapshots showing the underwater cooperative interaction between the robotic gripper and the untethered rolling robot protected by the living skin.

water-driven dimensional changes that would otherwise compromise the function of the protective layer. The mechanical robustness, softness, self-healing capability and waterproof nature of the mycelium-based living material provide robots with a protective skin that features several functionalities of biological animal skins. This proof-of-concept demonstration sets the stage for future research on the development of mycelium-based living skins for soft robots. Because the self-regeneration of the living skin requires nutrients,

printing of vascularized structures connected to an embedded nutrient source is a possible strategy to be further explored.

Outlook

Combining the livingness of microorganisms with the shaping capabilities of 3D-printing technologies is a powerful pathway towards the creation of functional living materials with unparalleled complex adaptive properties. Using this strategy, hydrogels loaded with the microorganisms of interest can be shaped into architectures that fulfil a functional design and also provide an adequate environment for growth of the biological species. The living properties of the resultant architectures emerge from the metabolic activity of the organisms embedded in the hydrogel. This metabolic activity imbues the mycelium-based living material with several hallmarks of complex adaptive systems, including the dissipative self-organization processes that enable growth and regeneration, the hierarchical organization of building blocks across multiple length scales, the optimal transport properties of scale-free fractal networks and the decision-making capabilities that emerge from the decentralized cooperative action of information-processing cells. The 3D printing of fungal hydrogels with such complex adaptive properties offers a unique opportunity to create functional mycelium-based living materials for several applications and can potentially inspire other strategies to bring life to the realm of materials.

Online content

Any methods, additional references, Nature Portfolio reporting summaries, source data, extended data, supplementary information, acknowledgements, peer review information; details of author contributions and competing interests; and statements of data and code availability are available at https://doi.org/10.1038/s41563-022-01429-5.

References

1. Speck, T. & Burgert, I. Plant stems: functional design and mechanics. *Annu. Rev. Mater. Res.* **41**, 169–193 (2011).
2. Florea, M. et al. Engineering control of bacterial cellulose production using a genetic toolkit and a new cellulose-producing strain. *Proc. Natl Acad. Sci. USA* **113**, E3431–E3440 (2016).
3. Di Giacomo, R., Daraio, C. & Maresca, B. Plant nanobionic materials with a giant temperature response mediated by pectin-Ca^{2+}. *Proc. Natl Acad. Sci. USA* **112**, 4541–4545 (2015).
4. Jonkers, H. M. in *Self Healing Materials: an Alternative Approach to 20 Centuries of Materials Science* (ed. van der Zwaag, S.) 195–204 (Springer Netherlands, 2007).
5. Gilbert, C. et al. Living materials with programmable functionalities grown from engineered microbial co-cultures. *Nat. Mater.* **20**, 691–700 (2021).
6. Gerber, L. C., Koehler, F. M., Grass, R. N. & Stark, W. J. Incorporating microorganisms into polymer layers provides bioinspired functional living materials. *Proc. Natl Acad. Sci. USA* **109**, 90–94 (2012).
7. Liu, X. et al. 3D printing of living responsive materials and devices. *Adv. Mater.* **30**, 1704821 (2018).
8. Duraj-Thatte, A. M. et al. Genetically programmable self-regenerating bacterial hydrogels. *Adv. Mater.* **31**, e1901826 (2019).
9. Schaffner, M., Ruhs, P. A., Coulter, F., Kilcher, S. & Studart, A. R. 3D printing of bacteria into functional complex materials. *Sci. Adv.* **3**, eaao6804 (2017).
10. Joshi, S., Cook, E. & Mannoor, M. S. Bacterial nanobionics via 3D printing. *Nano Lett.* **18**, 7448–7456 (2018).
11. Heveran, C. M. et al. Biomineralization and successive regeneration of engineered living building materials. *Matter* **2**, 481–494 (2020).
12. Lehner, B. A. E., Schmieden, D. T. & Meyer, A. S. A straightforward approach for 3D bacterial printing. *ACS Synth. Biol.* **6**, 1124–1130 (2017).
13. Kriegman, S., Blackiston, D., Levin, M. & Bongard, J. A scalable pipeline for designing reconfigurable organisms. *Proc. Natl Acad. Sci. USA* **117**, 1853–1859 (2020).
14. The Royal Society. Animate materials. https://royalsociety.org/topics-policy/projects/animate-materials/ (2021).
15. Nguyen, P. Q., Courchesne, N. M. D., Duraj-Thatte, A., Praveschotinunt, P. & Joshi, N. S. Engineered living materials: prospects and challenges for using biological systems to direct the assembly of smart materials. *Adv. Mater.* **30**, e1704847 (2018).
16. Mitchell, M. *Complexity: A Guided Tour* (Oxford Univ. Press, 2009).
17. Gow, N. A. & Gadd, G. M. *Growing Fungus* (Springer, 1995).
18. Andrews, J. H. *Comparative Ecology of Microorganisms and Macroorganisms* (Springer-Verlag, 2017).
19. Aleklett, K., Ohlsson, P., Bengtsson, M. & Hammer, E. C. Fungal foraging behaviour and hyphal space exploration in micro-structured Soil Chips. *ISME J.* **5**, 1782–1793 (2021).
20. Wösten, H. A. B. et al. How a fungus escapes the water to grow into the air. *Curr. Biol.* **9**, 85–88 (1999).
21. Holt, G. A. et al. Fungal mycelium and cotton plant materials in the manufacture of biodegradable molded packaging material: evaluation study of select blends of cotton byproducts. *J. Biobased Mater. Bioenergy* **6**, 431–439 (2012).
22. Heisel, F. et al. Design, cultivation and application of load-bearing mycelium components: the MycoTree at the 2017 Seoul Biennale of Architecture and Urbanism. *Int. J. Sustain. Energy Dev.* https://doi.org/10.20533/ijsed.2046.3707.2017.0039 (2017/18).
23. Haneef, M. et al. Advanced materials from fungal mycelium: fabrication and tuning of physical properties. *Sci. Rep.* **7**, 41292 (2017).
24. Jones, M., Gandia, A., John, S. & Bismarck, A. Leather-like material biofabrication using fungi. *Nat. Sustain.* **4**, 9–16 (2021).
25. Antinori, M. E. et al. Advanced mycelium materials as potential self-growing biomedical scaffolds. *Sci. Rep.* **11**, 12630 (2021).
26. Bigall, N. C. et al. Fungal templates for noble-metal nanoparticles and their application in catalysis. *Angew. Chem. Int. Ed.* **47**, 7876–7879 (2008).
27. Mizzi, L. et al. Assessing the individual microbial inhibitory capacity of different sugars against pathogens commonly found in food systems. *Lett. Appl. Microbiol.* **71**, 251–258 (2020).
28. Maurice, S. et al. Modelling the effect of temperature, water activity and pH on the growth of *Serpula lacrymans*. *J. Appl. Microbiol.* **111**, 1436–1446 (2011).
29. Fricker, M. D., Heaton, L. L. M., Jones, N. S. & Boddy, L. The mycelium as a network. *Microbiol. Spectr.* https://doi.org/10.1128/microbiolspec.FUNK-0033-2017 (2017).
30. O'Loughlin, P. F. et al. Selection and development of preclinical models in fracture-healing research. *J. Bone Jt Surg.* **90**, 79–84 (2008).

Methods

Materials

The following chemicals were purchased and used as received: malt extract (Sigma-Aldrich), peptone (Sigma-Aldrich), agar (Duchefa), κ-carrageenan (Acros Organics), maltodextrin (PanReac AppliChem), calcium sulfate ($CaSO_4$, Sigma-Aldrich), Sylgard 184 (Sigma-Aldrich) and calcofluor white (Sigma-Aldrich). A cellulose-based thickener (MCG, Vivapur MCG 811 P) was kindly provided by JRS Pharma. The fungal species *G. lucidum* (China strain number 112001) and beech wood sawdust were purchased from Tyroler Glückspilze.

Preparation of growth media and cell culture

Two types of growth media were prepared as feeding substrates for the fungus: malt extract agar (MEA) and wood chip substrate. MEA medium was prepared by adding 0–200 g l^{-1} (0–20%) malt extract, 5 g l^{-1} (0.5%) peptone and 16 g l^{-1} (1.6%) agar to water and adjusting the pH to 6.8 using 1 M NaOH and 1 M HCl. To obtain MEA plates, the medium was sterilized at 121 °C for 20 min in an autoclave (2840 EL, Tuttnauer) and, subsequently, poured into cell culture dishes and left to solidify. The wood-chip-based substrate was prepared by mixing 800 g beech wood sawdust with 8 g maltodextrin, 10 g calcium sulfate and 1 l distilled water. The mixture was placed into glass jars and autoclaved at 121 °C for 20 min.

The fungus was subcultured by placing a small slice of a MEA plate fully covered with mycelia onto a fresh growth plate (2% malt extract) every 3–5 weeks. The cultures were grown in the dark at 23 °C and 95% relative humidity.

Growth behaviour on agar plates

The growth of the fungus on agar-based substrates was evaluated by preparing MEA plates containing malt extract concentrations ranging from 0 to 20%. After placing an inoculum (1 × 1 cm^2) into the middle of the culture plate, samples were stored in the dark at 23 °C under 95% relative humidity and the radial expansion of the fungus was measured every day. The thickness of the mycelium layer was determined optically by cutting out a piece of the plate and observing its cross-section under an optical digital microscope (VHX-6000, Keyence).

Bridging of mycelia across air gaps

The ability of the mycelia to span gaps over air was determined by placing inoculated MEA plates at a well-defined distance from each other using customized polylactic acid sample holders made in a desktop 3D printer (Ultimaker 3). The sample holder contained two ledges separated by a deep gap to prevent the mycelia from simply growing on the surface between the MEA plates (Extended Data Fig. 8a–c). For the experiment, a piece of overgrown MEA substrate was placed on the ledge opposite a fresh substrate to create air gaps ranging from 0.5 mm to 6 mm. The samples were stored at 23 °C and 95% relative humidity and monitored every day to evaluate the growth of the mycelia across the air gap.

Preparation of mycelium inks

Mycelium inks for 3D printing were prepared using the same medium compositions used for the preparation of the MEA plates. The base growth medium consists of an aqueous solution containing 0–20% malt extract and 0.5% peptone at a pH of 6.8. To adjust the rheological properties of the base medium, the ink also contains 15 g l^{-1} (1.5%) agar, 15 g l^{-1} (1.5%) κ-carrageenan and 30 g l^{-1} (3%) cellulose-based thickener (MCG) pre-suspended in water. The suspension of the cellulose-based thickener was prepared by dispersing the MCG powder in deionized water using a high-shear mixer (T25 digital Ultra Turrax, IKA) for 5 min at 1,000 r.p.m. followed by another 5 min at 20,000 r.p.m. After a rest period of at least 15 minutes, the suspension was combined with the remaining ink components and autoclaved at 121 °C for 20 min. The sterilized and solidified hydrogel was fragmented into a microgranular gel by mechanical mixing using a dynamic mixer (A-302, AIMOSHI) equipped with a milk frother tip (SM 3590, Severin) at 5,000 r.p.m. for 1 min.

The ink was either used directly as a reference ink or inoculated with mycelia to create a mycelium-containing ink. The mycelium inks were inoculated by spreading the fresh ink in a cell culture dish and placing a fungi inoculum onto the ink surface. After 7–10 days at 23 °C and 95% relative humidity, the whole surface was covered with mycelia and the dense mycelium layer formed was removed. The inoculated ink remaining underneath was quickly mixed by hand and filled into the printing cartridge. Before printing, the cartridge was centrifugated (Z306, Hermle) at 663*g* for 2 min to remove any entrapped air.

Rheology of mycelium inks

The rheological behaviour of the inks before and after inoculation was characterized using a plate–plate geometry mounted on a strain- and stress-controlled rheometer (MCR 302, Anton Paar). Oscillatory shear tests were performed to measure the storage (G′) and loss (G″) moduli of the inks by applying amplitude sweeps at an angular frequency of 1 rad s^{-1} and frequency sweeps at 1% shear strain. The yield stress of the inks was determined by applying a stress-controlled deformation to the sample and measuring the resulting shear strain. The yield stress was arbitrarily taken as the stress required to achieve a plastic deformation of 5%. The elastic recovery of the inks was measured by applying a shearing protocol designed to partly simulate the printing conditions. In this protocol, the storage and loss moduli of the undisturbed ink was first probed by applying an oscillatory shear strain of 1% amplitude at 10 rad s^{-1}. Afterward, the material was subjected to steady shear at 1 s^{-1} and the apparent viscosity was measured. The elastic recovery of the ink was finally quantified by measuring the evolution of the storage and loss moduli of the ink through oscillatory measurements right after the steady shear was stopped. In addition to elastic recovery, the inks were also characterized in terms of flow behaviour under steady shear conditions. To this end, we measured the apparent viscosity of inks containing varying concentrations of malt extract and rheological modifiers at shear rates between 0.1 and 100 s^{-1}.

The 3D printing of mycelium inks

Grid structures were 3D printed using a desktop printer (Ultimaker 2+) modified to enable the deposition of hydrogel filaments via direct ink writing. For this purpose, the original print head was replaced by a custom-made extrusion system consisting of a mechanically driven syringe pump that can accommodate 25 ml syringes (Extended Data Fig. 8d,e). The print paths for the 3D-printed grid structures were designed using Grasshopper (Rhinoceros, Robert McNeel & Associates). The custom code enabled the 3D printing of grids with various sizes, nozzle diameters and print line distances. Typically, parts were printed onto sterilized glass substrates using a print-head velocity of 20 mm s^{-1} and the printer was operated inside a laminar flow hood. Unless otherwise stated, the grid samples were printed with a 0.84 mm nozzle and a line gap of 1.2 mm and were later grown for 10 days at 23 °C and 95% relative humidity. The printed structures were found to remain dimensionally stable under this high humidity (no swelling). Pictures of the grids after mycelial growth were taken using a Canon EOS 6D and a macro objective (EF 100 mm f/2.8L Macro IS USM, Canon). Cross-section images were obtained by cutting the sample in half using a razor blade.

Biomass of mycelium-containing grids

The biomass of printed grids containing mycelia was determined by extracting the material generated by the fungi during growth. To this end, the samples were first cut into small pieces and immersed in water. After shaking the samples in water for 5 minutes, the resulting suspension was filtered using a 100 µm woven wire mesh (stainless steel, Retsch) and rinsed with water to wash away any remaining ink components. The solid residue remaining in the mesh was weighed

and dried at 60 °C for 24 h before weighing again. The dry biomass was determined as the fraction of the dried mass with respect to the initial weight of the grid.

Mechanical compression tests

The mechanical properties of 3D-printed grid structures with a nominal size of 20 × 20 × 10 mm^3 were measured by performing uniaxial compression tests. The compression tests were carried out using a universal mechanical testing machine (AGS-X, Shimadzu) with a 100 N-capacity load cell by applying a constant displacement rate of 5 mm min^{-1}. The mechanical stiffness of the samples was taken at an arbitrarily applied strain between 24 and 26%. With the help of cyclic measurements, we found that the material shows reversible viscoelastic properties when compressed at such a strain value. The instantaneous stiffness data shown in the main text (Fig. 3) show the same trends irrespective of the arbitrarily chosen strain value.

Confocal microscopy of growing mycelia

Scanning laser confocal imaging was performed to study the growth of mycelia between two printed filaments separated by an air gap (Fig. 4a). The filaments were 3D printed using a mycelium ink containing 10 μg g^{-1} of calcofluor white to enable staining of the chitin molecules produced by the fungus. The ink was printed directly onto a No. 0 glass slide with a thickness of 130 μm and covered with another glass slide using polydimethylsiloxane frames as spacers (Sylgard 184). The polydimethylsiloxane frames acted as a vapour barrier to prevent drying of the samples, while also allowing for the diffusion of oxygen needed for cell growth. The samples were imaged using a scanning laser confocal microscope (TCS SP8, Leica) at ×20 magnification (HC PL Fluotar ×20/0.55, Leica). Fluorescence was induced using a 405 nm diode laser and then collected with a hybrid detector for wavelengths from 439 nm to 713 nm. For the time-lapse experiments, images with 512 × 2,812 × 80 pixels and a voxel size of 0.506 μm × 0.506 μm × 1.275 μm were captured every 25 minutes. Images are displayed as maximum *z* projections, where *z* is the vertical axis parallel to the incoming light. Image analysis was performed using Fiji image analysis software[31].

Self-healing of mycelium-based living materials

The self-healing behaviour of the mycelium-based living materials was first studied by performing tensile mechanical tests on fungi-containing grids printed in a dog-bone geometry (Fig. 4c,d). The grids were printed with a nozzle diameter of 0.84 mm, a line gap of 1.2 mm and a malt extract concentration of 10% in the ink. The dog-bone samples showed a transverse cross-section of 10 mm × 10 mm, a gauge length of 36 mm and an overall length of 60 mm between end tabs. The specimens were fixed by end tabs consisting of two aluminium meshes covering a core of inoculated wood chip substrate and spaced apart by metal nuts. The two metal end tabs were fixed together using aluminium bars to prevent the samples from deforming during mounting in the testing machine (Extended Data Fig. 6b). The metal bars were removed prior to testing and the samples were tested at a displacement rate of 10 mm min^{-1} using a universal mechanical testing machine with a 100 N-capacity load cell (AGS-X, Shimadzu). After fracture, the sample was returned to the initial distance and the aluminium bars reattached to enable self-healing of the fractured surfaces. Self-healing occurred by incubating the samples at 23 °C and a relative humidity of 95% for at least three days. Following the incubation period, the self-healed samples were tested again using the procedure described above. This procedure was repeated multiple times to characterize the mechanical properties of the sample after several fracture–healing events (Fig. 4c).

The self-healing ability of mycelium-covered films was investigated by deliberately cutting defects with increasing width into overgrown MEA plates (Fig. 4b). The films were prepared with malt extract concentrations varying from 0 to 20%. The self-healing ability of a film was characterized in terms of the length of mycelia that grew across the cut width.

Living skins for robotic gripper and rolling robots

A custom-built five-axis 3D printer (Stepcraft D-600 Gantry with ISEL ZDS 2030 Tilt Rotary Table) was equipped with a volumetric dispensing unit (eco-PEN 300, ViscoTec)[32] to create the living skins for the robotic gripper and the untethered rolling robots (Fig. 4f–i). The grid-like architecture used as a template for the skin was printed on non-planar mandrels that were fabricated from polylactic acid using a regular desktop 3D printer (Prusa mk3, Prusa). Multi-axis computer numerical control toolpaths were calculated, and the subsequent Machine GCodes were created in the visual programming environment Grasshopper3D. Such toolpath strategies were essential to ensure that the printer nozzle was maintained perpendicular to the surface of the substrate at all times during the course of the print, enabling a smooth and even coating. The living skins were formed after incubation of the as-printed grids at 23 °C and 95% relative humidity for seven days. The robotic gripper comprised a custom-made three-finger gripper mounted on a commercial robotic arm (X-arm 2.2, Lobot), whereas the rolling robots consisted of commercially available products in two distinct sizes (Bolt & Mini, Sphero). The living skin of the rolling robots was generated by covering the spherical robot with two mycelial grids with hemisphere shape (Fig. 4h) and joining them together through the air bridging of mycelia across opposite surfaces. Similarly, the skin for the fingers of the robotic gripper was assembled from half-shells, whereas flat grids were wrapped around the base of the robot and left to join for three days to form a continuous skin.

Contact angle measurements

The hydrophobic nature of the mycelium-based living skin was characterized by measuring the contact angle of water on the surface of a MEA plate covered with mycelia (Extended Data Fig. 9). Contact angle measurements were conducted using a drop shape analyser (DSA 100, Krüss). The analysed water droplets had a volume of 8 μl and were deposited at a dispensing rate of 20 μl min^{-1} using a 0.51 mm nozzle.

Scanning electron microscopy

Cross-sections of mycelium-covered grids were freeze-dried (FreeZone 2.5, Labconco) and imaged with a scanning electron microscope (Gemini 450, Zeiss) operated with an acceleration voltage of 3 kV. Prior to imaging, the samples were coated with a 5 nm Pt layer using a compact coating unit (CCU-010, Safematic).

Reporting summary

Further information on research design is available in the Nature Portfolio Reporting Summary linked to this article.

Data availability

Data generated or analysed during this study are available at Zenodo: https://doi.org/10.5281/zenodo.7212419. Further data are available from the corresponding authors upon request. Source data are provided with this paper.

Code availability

The Grasshopper files for print path generation are available at Zenodo: https://doi.org/10.5281/zenodo.7212419.

References

31. Schindelin, J. et al. Fiji: an open-source platform for biological-image analysis. *Nat. Methods* **9**, 676–682 (2012).
32. Coulter, F. B. et al. Bioinspired heart valve prosthesis made by silicone additive manufacturing. *Matter* **1**, 266–279 (2019).

Acknowledgements

We thank the Swiss Competence Center for Energy Research for funding in Capacity Area A3 on the minimization of energy demand

(K.M. and A.R.S.). We are greateful for Swiss National Science Foundation Consolidator grant BSCGIO_157696 (S.G., F.B.C. and A.R.S.). We thank the Swiss National Science Foundation for funding within the framework of the National Center of Competence in Research for Bio-Inspired Materials (P.A.R. and A.R.S.).

Author contributions

The conceptualization was by S.G., P.A.R., K.M. and A.R.S. The methodology was by S.G., E.C., J.K., E.T., F.B.C., K.M. and P.A.R. The software was by S.G. and F.B.C. The investigation was by S.G., E.C., J.K., E.T., F.B.C., K.M. and P.A.R. The visualization was by S.G., E.C. and J.K. Funding acquisition was by A.R.S. Project administration was by S.G. Supervision was by S.G., K.M., P.A.R. and A.R.S. Writing the original draught was done by S.G. and A.R.S. Reviewing and editing the paper was done by S.G., K.M., P.A.R., F.B.C. and A.R.S.

Competing interests

The authors declare no competing interests.

Additional information

Extended data is available for this paper at https://doi.org/10.1038/s41563-022-01429-5.

Supplementary information The online version contains supplementary material available at https://doi.org/10.1038/s41563-022-01429-5.

Correspondence and requests for materials should be addressed to Kunal Masania or André R. Studart.

Peer review information *Nature Materials* thanks Athanassia Athanassiou, Alexander Bismarck, Wil Srubar III and the other, anonymous, reviewer(s) for their contribution to the peer review of this work.

https://doi.org/10.1038/s41563-022-01429-5

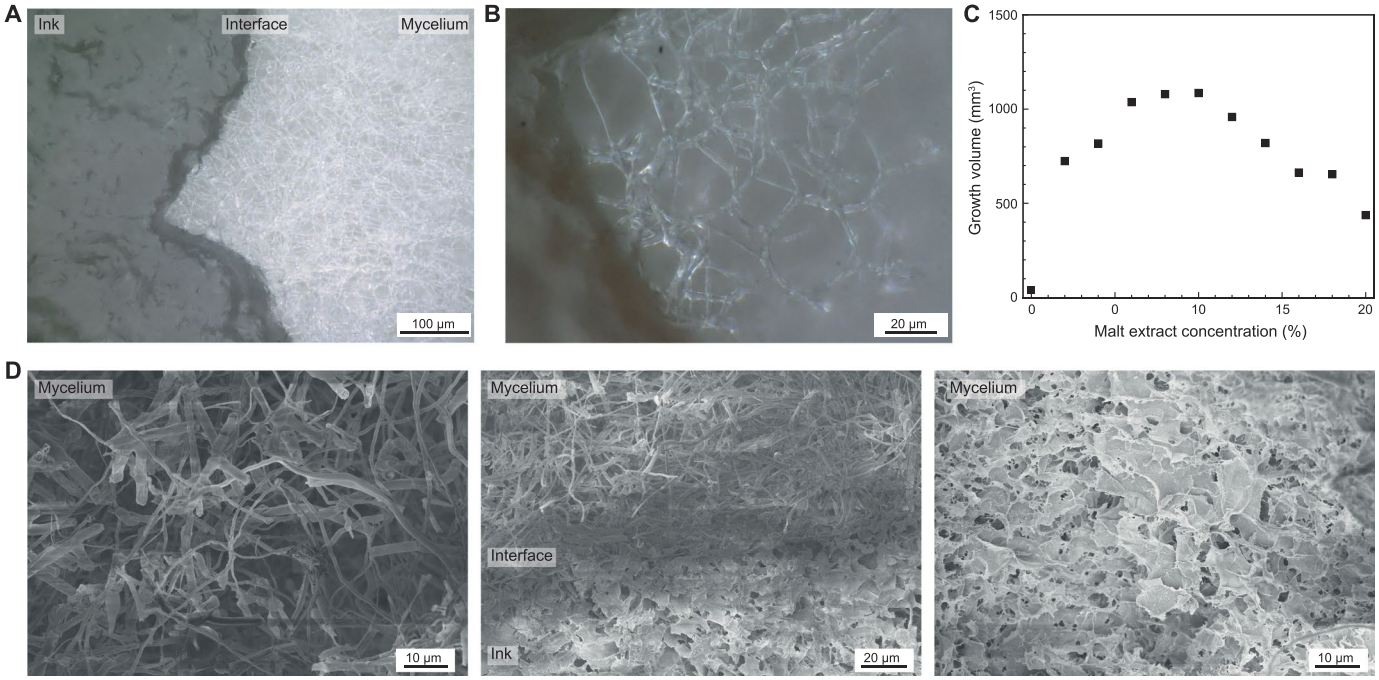

Extended Data Fig. 1 | Mycelium growth within hydrogel grid. (**A, B**) Optical microscopy images of a cross-sectional cut of a 3D grid printed from an ink containing 10% malt extract concentration. The images show the mycelium growth on the surface of the ink. (**C**) Estimated volume of the mycelium layer grown on agar hydrogels. The volume was calculated from the radius and thickness of the grown mycelium network (Fig. 2B). (**D**) Scanning electron microscopy images showing the freeze-dried structure of mycelium grown on a printed hydrogel filament. The images shown in (A,B,D) are representatives of a series of 3 equal experiments.

https://doi.org/10.1038/s41563-022-01429-5

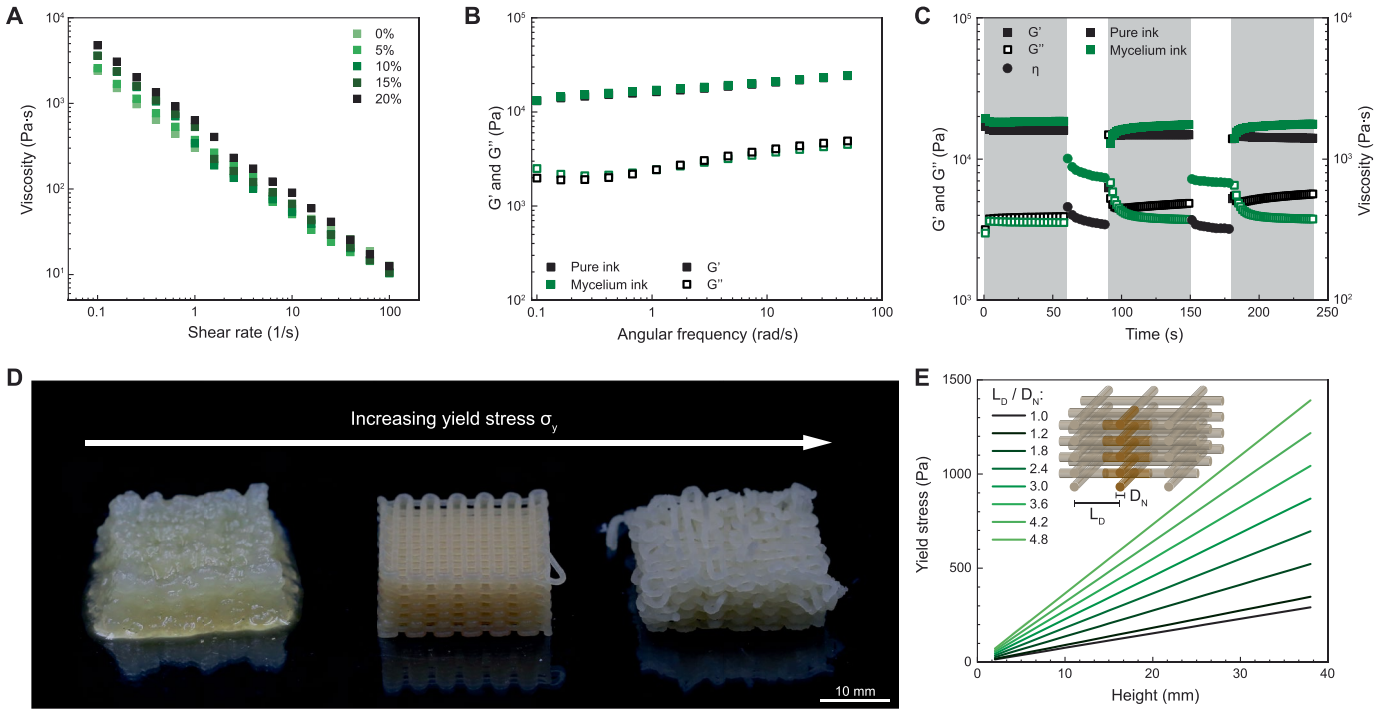

Extended Data Fig. 2 | Rheological properties and printability of mycelium inks. (**A**) Apparent viscosity of hydrogel inks measured under steady shear conditions, indicating the shear thinning behaviour of inks containing varying concentrations of malt extract. (**B**) Storage (G') and loss (G') moduli of inks before and after inoculation obtained from oscillatory rheological measurements at increasing applied frequency. The data show that the printed inks are predominantly elastic over the entire range of probed frequencies. (**C**) Rheological response of inks under printing simulation conditions. The alternating oscillatory (grey area) and steady-state (white area) measurements show quick recovery of the storage modulus of the ink upon cessation of shear. (**D**) 3D printed grids obtain from inks with increasing yield strength of approximately 100 Pa (left) 400 Pa (middle) and >1000 Pa (right). The images indicate filament sagging and flowing for inks with low yield stress, whereas high-yield-stress inks lead to fragile and brittle grids. Optimal print results are achieved with inks at intermediate yield stress level. (**E**) Effect of height and line gap spacing on the minimum yield stress required to print hydrogel grids that resist gravity-induced distortion. L_D and D_N correspond to the line spacing and the filament diameter, respectively.

https://doi.org/10.1038/s41563-022-01429-5

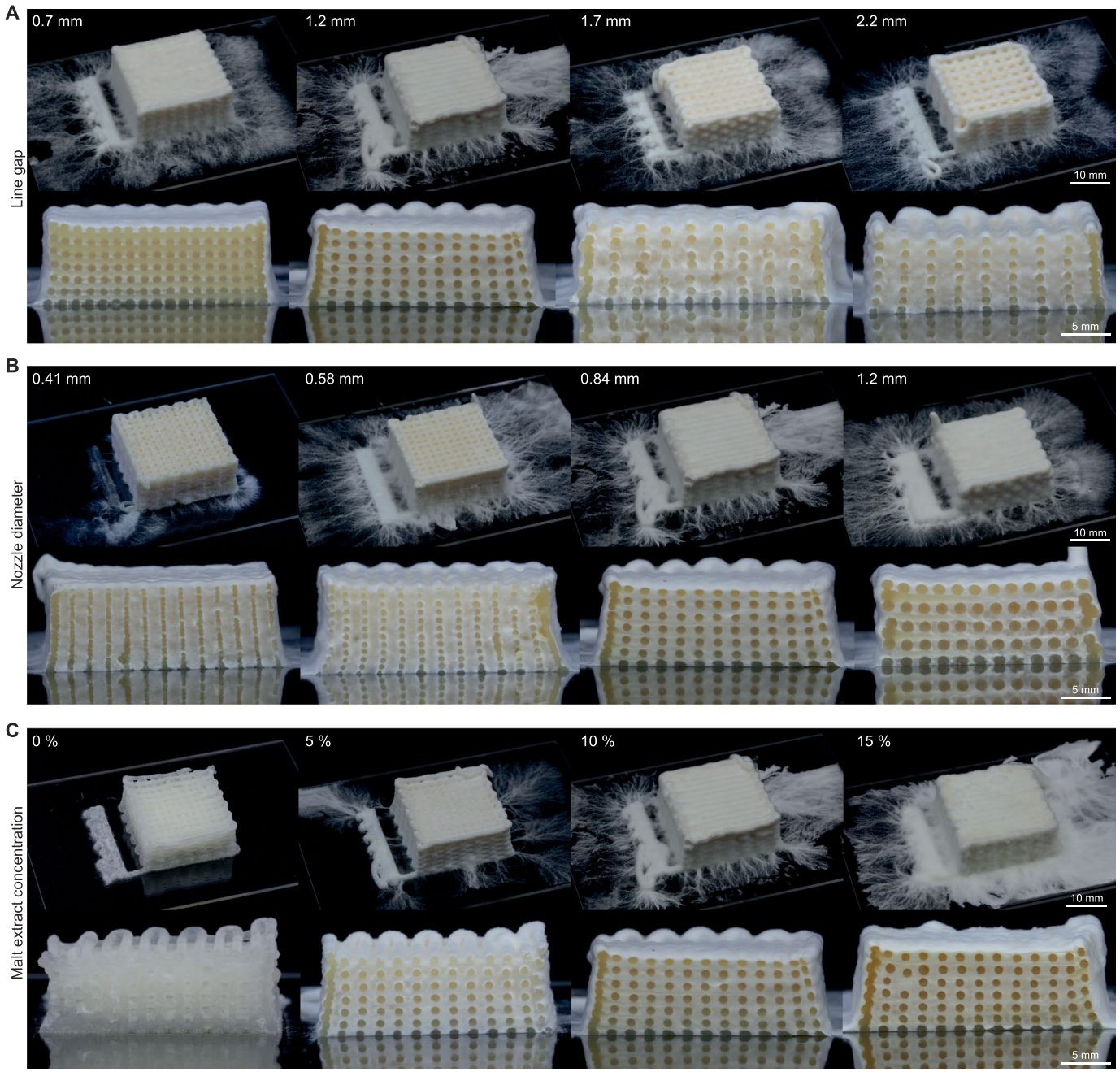

Extended Data Fig. 3 | 3D printed mycelium grid structures. (**A-C**) Photographs of grids after 10 days of growth for structures printed with varying (A) line gaps, (B) nozzle diameters, and (C) malt extract concentrations.

https://doi.org/10.1038/s41563-022-01429-5

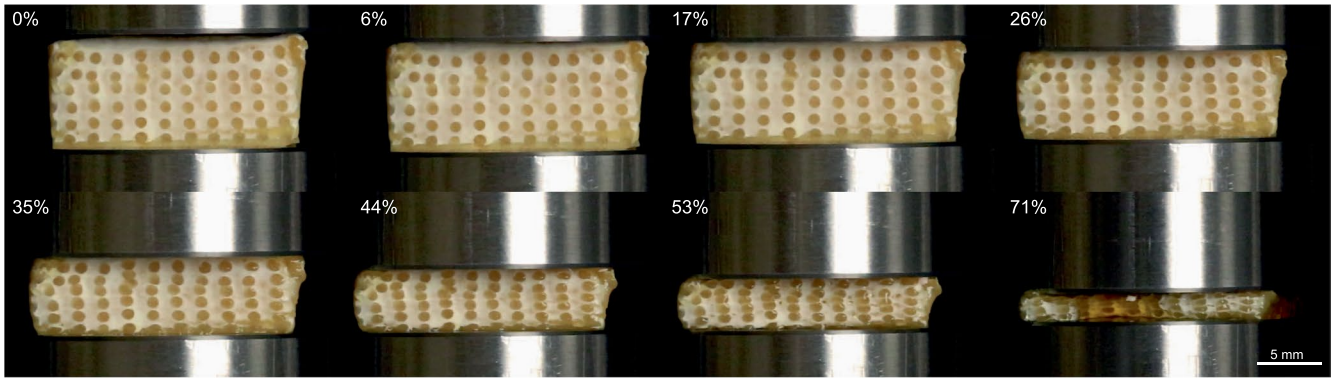

Extended Data Fig. 4 | Mycelium grid structure during compression testing. Snapshots taken at distinct compressive strains show the changing internal structure of the material. The grids were printed from inks containing 10 % malt extract with a line gap of 1.2 mm and nozzle diameter of 0.84 mm.

https://doi.org/10.1038/s41563-022-01429-5

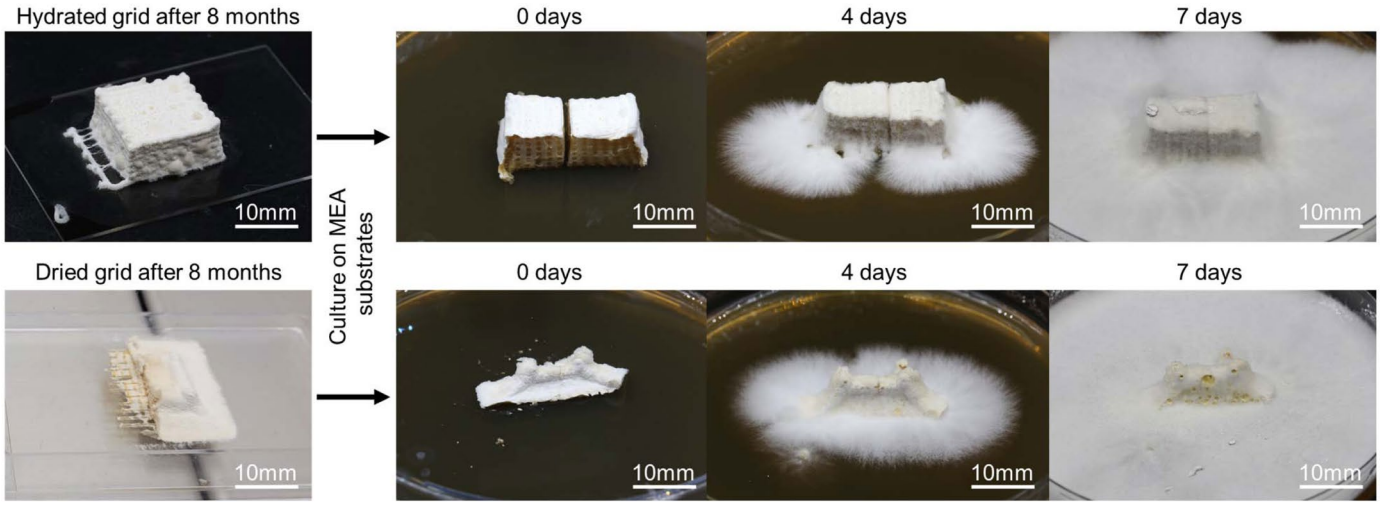

Extended Data Fig. 5 | Long-term resilience and biological viability of mycelia-based structures. Printed living grids that were maintained hydrated (upper row) or dried (lower row) for 8 months are able to re-grow the mycelial network after culturing on malt extract growth plates. Both samples quickly regenerated new mycelium and colonized the plates within 7 days of growth.

https://doi.org/10.1038/s41563-022-01429-5

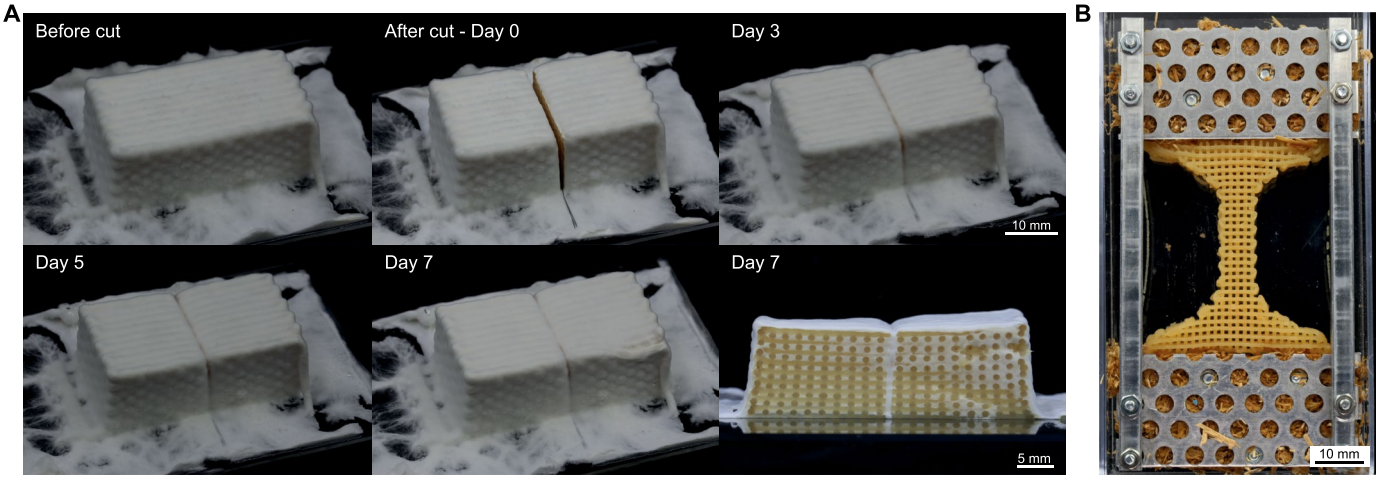

Extended Data Fig. 6 | Self-healing of cuts made in the printed mycelium grids. (**A**) A 3D printed grid was intentionally cut and imaged for a duration of 7 days. After this time period, the cross-section image of the sample shows that the cut is fully healed through the growth of mycelia across the open space. (**B**) Setup comprising metal frame and wood chip substrate used to evaluate the tensile mechanical properties and self-healing ability of printed mycelium grids.

https://doi.org/10.1038/s41563-022-01429-5

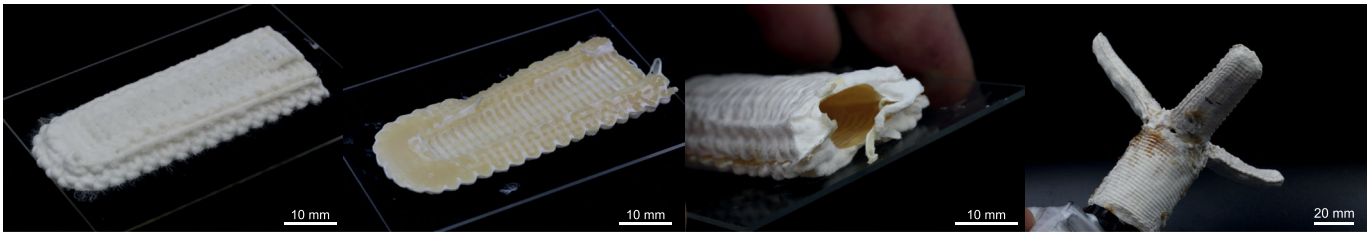

Extended Data Fig. 7 | Strategy to fabricate the mycelium-based skin for the robotic gripper. From left to right: non-planar 3D printed half of the robotic skin after 7 days of growth. Counterpart flipped to show the bottom side of the printed structure. The two halves put together ready to mount onto the mechanical actuators. Final mycelium-based skin assembled around the gripper after an additional 3 days of growth to fuse the individual parts together.

https://doi.org/10.1038/s41563-022-01429-5

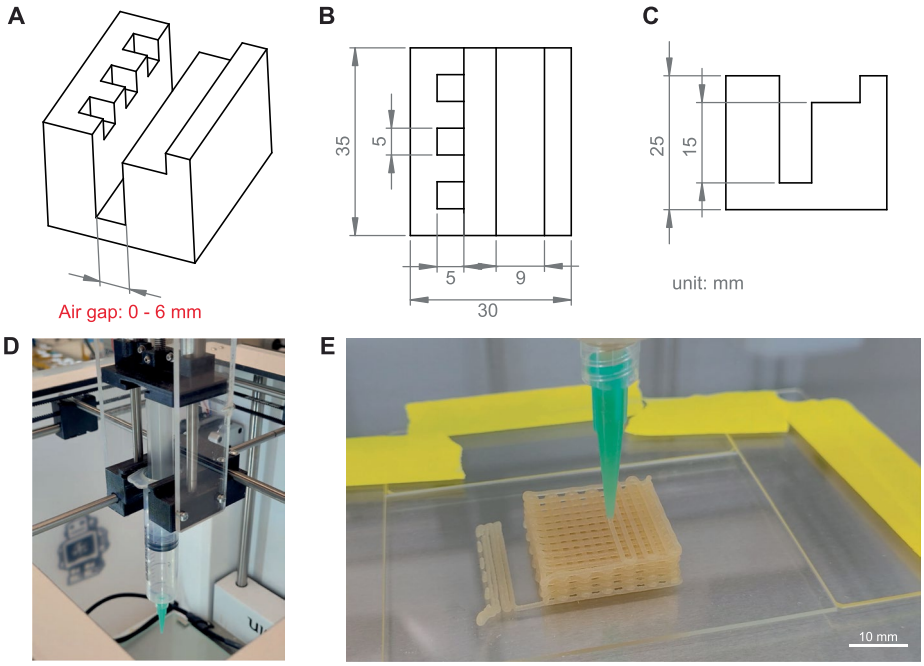

Extended Data Fig. 8 | Sample holder used for bridging experiments and 3D printing setup. (**A**) 3D representation indicating the air gap that was changed to create a distance for the mycelium to bridge. (**B,C**) Drawings displaying different cross-sections of the sample holder. (**D**) Custom-built syringe pump mounted on a fused filament fabrication printer (Ultimaker 2+) to create the direct ink writing setup (DIW). (**E**) DIW of the mycelium ink into a grid structure.

https://doi.org/10.1038/s41563-022-01429-5

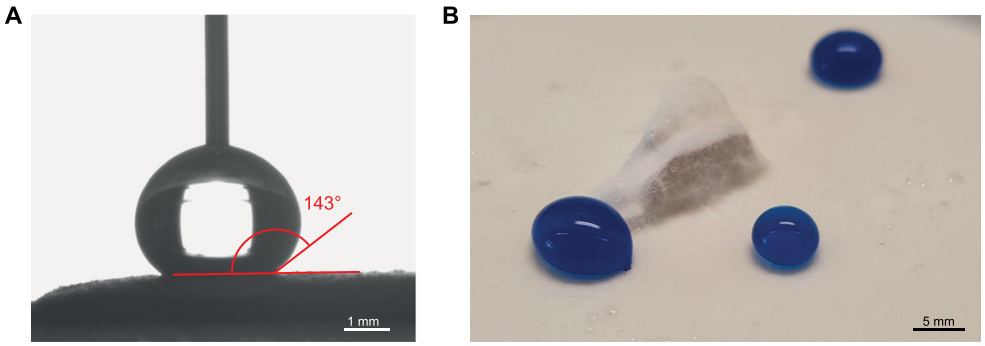

Extended Data Fig. 9 | Surface hydrophobicity of printed structures. (**A**) Contact angle measurement on a mycelium-covered surface. (**B**) Colored water droplets on a plate covered with mycelium.

https://doi.org/10.1038/s41563-022-01429-5

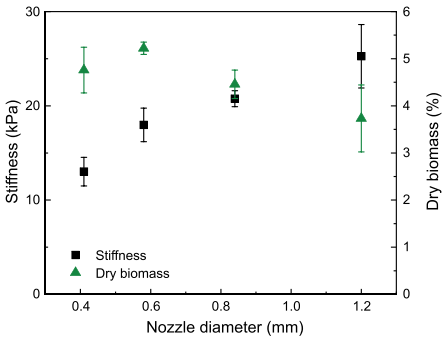

Extended Data Fig. 10 | Effect of nozzle diameter on the dry biomass and stiffness of mycelium grids. Apparent mechanical stiffness and biomass content of mycelia-laden grids printed with varying nozzle diameters. The line distance and the malt extract concentration were kept constant at 2 mm and 10%, respectively. The apparent stiffness values reported correspond to the instantaneous elastic modulus at a strain value of 25%. The data represent the mean values and the standard deviation obtained from 5 measurements of distinct samples at each data point.

nature portfolio

Corresponding author(s): André R Studart

Last updated by author(s): Jul 5, 2022

Reporting Summary

Nature Portfolio wishes to improve the reproducibility of the work that we publish. This form provides structure for consistency and transparency in reporting. For further information on Nature Portfolio policies, see our Editorial Policies and the Editorial Policy Checklist.

Statistics

For all statistical analyses, confirm that the following items are present in the figure legend, table legend, main text, or Methods section.

n/a	Confirmed	
☐	☒	The exact sample size (*n*) for each experimental group/condition, given as a discrete number and unit of measurement
☐	☒	A statement on whether measurements were taken from distinct samples or whether the same sample was measured repeatedly
☒	☐	The statistical test(s) used AND whether they are one- or two-sided *Only common tests should be described solely by name; describe more complex techniques in the Methods section.*
☒	☐	A description of all covariates tested
☒	☐	A description of any assumptions or corrections, such as tests of normality and adjustment for multiple comparisons
☐	☒	A full description of the statistical parameters including central tendency (e.g. means) or other basic estimates (e.g. regression coefficient) AND variation (e.g. standard deviation) or associated estimates of uncertainty (e.g. confidence intervals)
☒	☐	For null hypothesis testing, the test statistic (e.g. *F*, *t*, *r*) with confidence intervals, effect sizes, degrees of freedom and *P* value noted *Give P values as exact values whenever suitable.*
☒	☐	For Bayesian analysis, information on the choice of priors and Markov chain Monte Carlo settings
☒	☐	For hierarchical and complex designs, identification of the appropriate level for tests and full reporting of outcomes
☒	☐	Estimates of effect sizes (e.g. Cohen's *d*, Pearson's *r*), indicating how they were calculated

Our web collection on statistics for biologists contains articles on many of the points above.

Software and code

Policy information about availability of computer code

Data collection	Rhino3D Version 7 with Grasshopper3D Plugin Version 1.0.00007 was used to generate the custom (3 and 5 Axis) 3D printer tool-path code and associated material flow control signals. Fiji version 1.5c was used to generate maximum z-projection of acquired confocal images.
Data analysis	Data analysis was performed using MATLAB (R2019a)

For manuscripts utilizing custom algorithms or software that are central to the research but not yet described in published literature, software must be made available to editors and reviewers. We strongly encourage code deposition in a community repository (e.g. GitHub). See the Nature Portfolio guidelines for submitting code & software for further information.

Data

Policy information about availability of data

All manuscripts must include a data availability statement. This statement should provide the following information, where applicable:

- Accession codes, unique identifiers, or web links for publicly available datasets
- A description of any restrictions on data availability
- For clinical datasets or third party data, please ensure that the statement adheres to our policy

The datasets generated during and/or analyzed during the current study, as well as the Grasshopper files for print path generation, are available at https://doi.org/10.5281/zenodo.7212419

Human research participants

Policy information about studies involving human research participants and Sex and Gender in Research.

Reporting on sex and gender	NA
Population characteristics	NA
Recruitment	NA
Ethics oversight	NA

Note that full information on the approval of the study protocol must also be provided in the manuscript.

Field-specific reporting

Please select the one below that is the best fit for your research. If you are not sure, read the appropriate sections before making your selection.

☒ Life sciences ☐ Behavioural & social sciences ☐ Ecological, evolutionary & environmental sciences

For a reference copy of the document with all sections, see nature.com/documents/nr-reporting-summary-flat.pdf

Life sciences study design

All studies must disclose on these points even when the disclosure is negative.

Sample size	A standard sample size of 5 samples per test condition as used in mechanical analysis was used whenever possible.
Data exclusions	No data was excluded from the evaluation.
Replication	To ensure replicability of the data, media composition and growth duration kept consistent.
Randomization	No sample randomization was performed during this study. No statistical tests performed
Blinding	No blinding was done or possible due to temporal distributed data acquisition and optical clear optical differences between samples.

Reporting for specific materials, systems and methods

We require information from authors about some types of materials, experimental systems and methods used in many studies. Here, indicate whether each material, system or method listed is relevant to your study. If you are not sure if a list item applies to your research, read the appropriate section before selecting a response.

Materials & experimental systems

n/a	Involved in the study
☒	☐ Antibodies
☒	☐ Eukaryotic cell lines
☒	☐ Palaeontology and archaeology
☒	☐ Animals and other organisms
☒	☐ Clinical data
☒	☐ Dual use research of concern

Methods

n/a	Involved in the study
☒	☐ ChIP-seq
☒	☐ Flow cytometry
☒	☐ MRI-based neuroimaging